Preferred orientation of experimentally deformed pyrite measured by means of neutron diffraction

H. SIEMES AND D. ZILLES

Institut für Mineralogie und Lagerstättenlehre, RWTH Aachen, 5100 Aachen, Germany

S. F. COX

Research School of Earth Sciences, Australian National University, Canberra ACT 2601, Australia

P. MERZ, W. SCHÄFER AND G. WILL

Mineralogisches Institut, Universität Bonn, Außenstelle Forschungszentrum Jülich (KFA), 5170 Jülich, Germany

H. SCHAEBEN

Laboratoire de Metallurgie des Materiaux Polycristallins (LM2P), Universite de Metz, 57045 Metz, France

AND

K. KUNZE

Brigham Young University, Dept. of Manufacturing Engineering, Provo, UT 84602, USA

Abstract

Neutron diffraction texture goniometry indicates that naturally deformed polycrystalline pyrite ores from Mt. Lyell (Tasmania) and Degtiarka (Ural Mountains) have weak lattice preferred orientations. During experimental deformation involving dislocation flow at elevated temperatures and pressures, these initial fabrics have been modified to produce new lattice preferred orientations.

Polycrystalline pyrite form Mt. Lyell (B-1) has an initial <111>-fibre texture perpendicular to a grain-size layering. After 24% shortening perpendicular to the <111>-fibre axis at 700 °C, a new, but weak <100> texture has developed parallel to the shortening axis. The Degtiarka pyrite (PN-6) initially has two weak fibre components. The somewhat stronger component is a <100>-fibre texture, similar to that in the experimentally deformed B-1 pyrite. The other one is a <111>-fibre texture similar to the intital B-1 preferred orientation. After 30% shortening oblique to both initial fibre axes at 600 °C, weak <110>- and <111>-fibre textures have developed. The experimentally produced fabrics have developed during deformation involving dislocation flow, dynamic recrystallisation and some microcracking. Intergranular sliding may also have been involved. Differences between lattice preferred orientations developed in the 600 °C and 700 °C experiments are interpreted to indicate a change in the dominant flow mechanism with changing temperature.

In comparison with other cubic minerals that have been deformed experimentally by dislocation flow mechanisms, the pyrite shows an unusually weak preferred orientation which can be detected only by means of neutron diffraction texture goniometry.

KEYWORDS: pyrite, experimental deformation, neutron texture goniometry, preferred orientation, orientation distribution function.

Introduction

INVESTIGATION of naturally deformed polycrystalline pyrite from different locations by means of X-ray texture goniometry has shown that there is usually no preferred orientation recognisable (see review by Siemes and Hennig-Michaeli, 1985). Incomplete unnormalised pole figures of polycrystalline pyrite ore from the Bayerland mine were interpreted by Gehlen (1971) to indicate a preferred alignment of <111> parallel to the normal of a metamorphic layering.

Mineralogical Magazine, March 1993, Vol. 57, pp. 29–43

In triaxial compression tests, cylinders of polycrystalline pyrite 12 mm long and 7 mm in diameter have been shortened up to 30% by Cox *et al.* (1981). Because optical and TEM microstructural studies indicated that deformation has apparently occurred predominantly by dislocation flow mechanisms it seemed worthwhile to analyse the preferred orientation that developed in a number of specimens. Surprisingly, Zilles (1989) could only detect in some of the incomplete X-ray pole figures rather uncertain and inconsistent indications of preferred orientation. Assuming an average grain diameter of 50 μm, the irradiated sample area of approximately 25 mm^2 contains 10^4 grains. It was concluded that the irradiated area as well as as the number of grains was too small for a thorough texture analysis of a very weak preferred orientation. Therefore the central parts of two experimentally undeformed and two experimentally deformed specimens were analysed by neutron diffraction texture goniometry (Will *et al.*, 1989). With neutron diffraction, the total volume of the specimen (240 mm^3 with approx. 2.10^6 grains) is irradiated and contributes to the measured complete pole figures.

Deformation microstructures and mechanisms in experimentally deformed pyrite

Single crystal strength data, structural considerations and transmission electron microscopy studies suggest that above 400 °C {100} <001> and possibly {100} <011> are important slip modes in pyrite that has been experimentally deformed at strain rates between 10^{-4} s^{-1} and 10^{-5} s^{-1} (Cox *et al.*, 1981; Graf *et al.*, 1981; Levade *et al.*, 1982). Couderc *et al.* (1980) have also recognised the operation of {100} <001> glide in naturally deformed pyrite from Degtiarka. During <100> shortening of single crystals, a {110} glide system is also inferred to have operated, but has a critical resolved shear stress higher than for {100} glide (Cox, 1987). In comparison to other cubic minerals (Table 1) pyrite is quite unique because of the predominant glide mode {100} <001>.

Between 450 °C and 550 °C dislocation flow give rise to a weak grain elongation foliation, latttice bending, and deformation band development at strains up to about 20% shortening. Above about 550 °C grain boundary migration and dynamic recrystallisation also become important, with recrystallisation occurring by a combination of grain boundary bulging and subgrain rotation mechanisms (Cox *et al.*, 1981, and Cox, 1987).

Prefered orientation in shortening tests

Because of the axial symmetry of the experimental deformation process one expects the development of a fibre texture, that is a preferred orientation with a rotation axis of infinite order parallel to the axis of compression. That means that there develops a preferred orientation with an alignment of one (or two crystallographic direction(s) parallel to this axis. A lattice plane perpendicular to this crystallographic direction gives rise to a circular maximum in the centre of the pole figure. All other lattice planes have continuous pole density distributions on circles around the centre of the pole figures. If the undeformed specimens are inhomogenous or intially have a preferred orientation then the final pole density on the circles deviates from perfect axial symmetry. The density of the maximum in the fibre axis (expressed in multiples of uniform density, m.u.d.) is used as a measure of preferred orientation. Natural ores can have axisymmetric components of preferred orientation with different orientated fiber axes. These can originate by oriented grain growth or coaxial deformation paths.

Cubic minerals such as halite, galena, fluorite, sphalerite, and magnetite have slip modes with {100}, {110} and {111} as glide planes and <011> as glide directions. In Table 1 the glide modes are ordered according to their importance, that is with increasing relative critical resolved shear stresses (see review for sulfide and oxide minerals by Siemes and Hennig Michaeli, 1985, for galena by Foitzik *et al.*, 1991, for halite by Carter and Heard, 1970, and for fluorite by Pratt *et al.*, 1966). In all these crystals one slip mode or a combination of several of them yield five independent slip systems which allow a general deformation without volume change (Mises, 1928; Kelly and Groves, 1970). During uniaxial shortening, fibre textures develop such that <110> is aligned with the axis of compression (Table 1). Only halite exhibits two fibre components; the most predominent being again <110> the minor component being <100> (Kern and Braun, 1973). Both components are found in naturally deformed halites (Kämpf *et al.*, 1987; Kern and Richter, 1985). Cubic face-centered metals (Al, Cu, Ni) develop predominantly the <110>-fibre with a spread to <100> and <311> (Barrett and Levenson, 1940). All these orientations are such that several slip systems have high resolved shear stresses with reference to the maximum principal stress. The slip modes of pyrite are quite different from those of other cubic minerals, because the major slip modes yield only 3 independent slip systems. In an

TABLE 1. Preferred orientation of polycrystalline cubic crystals in axial symmetric shortening tests

Crystal structure glide modes	Max. exp. temp. °C	Max. strain %	Fibre axis	Reference
Halite	200	21	<110>	Kern and Braun, 1973
sodium chloride *Fm3m*			<100>	
{1 1 0} <1-1 0> slip				
{1 0 0} <0 1 1> slip				
{1 1 1} <1-1 0> slip				
Galena	25	36	<110>	Siemes, 1970, 1976
sodium chloride *Fm3m*	300	16		Siemes and Hennig-Michaeli, 1985
{1 0 0} <0 1 1> slip				
{1 1 0} <1-1 0> slip				
{4 4 1} <1 1-8> twinning				
Fluorite	25	14	<110>	Lang, 1968
fluorite *Fm3m*				
{1 0 0} <0 1 1> slip				
{1 1 0} <1-1 0> slip				
Sphalerite	25	20	<110>	Saynisch, 1970
sphalerite *F43m*	300	10		Kollenberg and Siemes, 1983
{1 1 1} <1-1 0> slip				
{1 1 1} <1 1-2> twinning				
Magnetite	300	20	<110>	Müller and Siemes, 1972
spinel *Fd3m*				
{1 1 1} <1-1 0> slip				
{1 0 0} <0 1 1> slip				
{1 1 0} <1-1 0> slip				
{1 1 1} <1 1-2> twinning				
Metal		98	<110> with spread to <311>, <100>	Barrett and Levenson, 1940
cubic face centred *Fm3m*				
{1 1 1} <1-1 0> slip				
Pyrite	600	30	<110>	Present work
sodium chloride			<111>	
derivative *Pa3*	700	24	<100>	
{1 0 0} <0 01 0> slip				
{1 0 0} <0 1 1> slip				
{1 1 0} < ? > slip				

orientation with <100> parallel to the axial stress the major glide systems have zero shear stresses. All the glide directions are either parallel or perpendicular to the stress axis. Therefore additional mechanisms must be activated, e.g. the {110} slip mode or microcracking or grain boundary sliding. By analogy one should expect for axial symmetric deformation of pyrite only fibre textures with an alignment of <110> and probably <111> parallel to the shortening axis.

Measurement and analysis of preferred orientation

Eight complete pole figures (pole density functions, PDFs) of the reflections (111), (200), (210), (220), (222), (211), (311), and (321) were measured on the pyrite specimens by neutron diffraction goniometry (Will *et al.*, 1989). The information which is presented in different pole figures is combined by means of pole figure inversion algorithms (e.g. Bunge and Esling, 1985; Matthies, 1991; Pawlik *et al.* 1991; Schaeben and Siemes, 1991; Vadon and Heizmann, 1991) to an orientation distribution function (ODF). From the measured pyrite reflections the (200)-, (220)- and (111)-pole figures were used to calculate a MENTEX-ODF according to the inversion method involving finite series expansion and entropy optimisation (Schaeben, 1988; Schaeben *et al.*, 1990; Schaeben, 1991). Table 2 summarises the results after 22 iterations. The mean relative errors (Table 2) and comparison of the experimental pole figures with the recalcu-

TABLE 2. Calculation of the ODFs by means of *m*aximum *en*tropy *tex*ture program MENTEX, 3 pole figures: (111), (200), (220), 22 interactions

	ODF m.u.d.		(111) PDF m.u.d.			(200 PDF m.u.d.			(220) PDF m.u.d.		
	min.	max.	min.	max.	RPO	min.	max.	RPO	min.	max.	RPO
Mt. Lyell, undeformed: B-1											
exp.:			0.73	1.24		0.81	1.22		0.78	1.18	
calc.:	0.71	1.87	0.83	1.20	3.06	0.80	1.18	2.66	0.88	1.19	3.07
Mt. Lyell, deformed: RUN 053											
exp.:			0.84	1.18		0.76	1.28		0.89	1.11	
calc.:	0.73	1.94	0.86	1.15	4.65	0.82	1.30	2.49	0.88	1.08	2.34
Degtiarka, undeformed: PN-6											
exp.:			0.68	1.31		0.71	1.44		0.85	1.14	
calc.:	0.65	1.81	0.72	1.26	3.22	0.71	1.36	3.81	0.89	1.15	1.74
Degtiarka, deformed: RUN 092											
exp.:			0.77	1.29		0.64	1.31		0.84	1.22	
calc.:	0.60	2.03	0.77	1.27	4.10	0.63	1.30	4.40	0.89	1.23	3.02

ODF: orientation distribution function, PDF: pole density function (= pole figure), m.u.d.: multiples of uniform density, exp.: experimental data, calc.: calculated data, RPO: mean relative error in percent

lated pole figures prove the MENTEX-ODF to be a reasonable approximation. The ODFs are presented in sigma sections (Matthies *et al.*, 1990*a*). Compared to the traditional plotting of ODF data in rectangular arrangements (Bunge, 1985), sigma sections provide an easier visulisation of preferred orientations. The series of sigma sections can be interpreted as a spread (001)-pole figure. Each section contains the density distribution for all crystal orientations with a constant $2\sigma = (\alpha = \gamma)$ in dependence on azimuth α and pole distance β, where α (rotatation about the crystal z-axis) β (rotation about the crystal y-axis) and γ (rotation about the crystal z-axis) are the Euler angles of an orientation. An arbitrary point (α, β) within a 2σ-section immediately gives the direction of the (001)-crystal axis of that orientation with reference to the specimen axes. Orientations at the same position (α, β) but with different sections $2\sigma_1$ and $2\sigma_2$ only differ in a rotation about that common axis through the angle $2*(\sigma_1-\sigma_2)$. Finally, the average distribution of all sigma sections is identical to the recalculated (001)-pole figure. The preferred orientations displayed in the pole figures and ODFs sigma sections were modelled by mathematical standard distributions by means of programs which have been developed at Rossendorf (Matthies *et al.*, 1987, 1988*a*, 1990*b*; Matthies *et al.*, 1988*b*). The models give a simplified impression of the main features of the measured pole figures and the calculated orientation distributions, and can be described by a small number of characteristic parameters (Table 3).

Pyrite from Mt. Lyell

The polycrystalline material (B-1) from the Blow orebody of the Mt. Lyell Mining and Railway Company near Queenstown, Tasmania, exhibits some compositional and grain size layering with grain sizes between 50 and 70 μm. The specimen cylinders were drilled parallel to the layering. Fig. 1*a* shows the pole figures of the three reflections (200), (220), and (111). In Fig. 1*b* the recalculated pole figures and in Fig. 2*a* the ODF in sigma sections are presented. Because of the good correspondence of the experimental and recalculated pole figures and the small mean relative errors (Table 2) the ODF provides reliable information about the preferred orientation. The pole figures and sigma sections are projected parallel to the cross section of the specimen and perpendicular to the layering of the ore. The pole figure shows a (111)-maximum perpendicular to the long axis of the specimen and a (111)-girdle in the plane of the layering. The associated fibre axis is oriented perpendicular to the layering and the preferred orientation is very weak because this maximum has a density of 1.24 m.u.d. (Table 2) that is close to randomness. Fig. 1*c* shows the modelled pole figures and Fig. 2*b* the related mathematical ODF-sections which confirm the interpretion as fibre texture.

The deformation of this pyrite at a strain rate of $2*10^{-4}$ s^{-1}, a temperature of 700 °C and at a confining pressure of 300 MPa (RUN 053, Cox *et al.*, 1981) occurred at a steady state stress difference of around 120 MPa up to 30% strain.

FIG. 3. Fibre components of textures of the pyrite ores

fibre axis	position of the fibre axis		mathematical model ODF		
	azimuth	pole angle	uniform portion	Gauss shaped distrib. portion	half-width
Mt. Lyell, undeformed: B-1					
<111>	302°	90°	70%	30%	40.0°
Mt. Lyell, deformed: RUN 053					
<100>	0°	0°	70%	30%	40.0°
Degtiarka, undeformed: PN-6					
<111>	262°	35°	70%	15%	40.0°
<100>	0°	35°		15%	40.0°
Degtiarka, deformed: RUN 092					
<111>	262°	35°	60%	7.5%	40.0°
<100>	0°	35°		7.5%	40.0°
<111>	195°	10°		12.5%	35.0°
<110>	0°	0°		12.5%	35.0°

ODF: orientation distribution function

Dislocation creep was accompanied by dynamic recrystallisation and the resulting development of a population of finer new grains. These are typically 10–15 μm in diameter and concentrated at the boundaries of original host grains. Fig 3*a* shows the pole figures of the (200)-, (220)- and (111)-reflections which are projected in the same orientation as those of the undeformed specimen. The deformation has induced a new weak fibre texture with a (100)-maximum (1.28 m.u.d.) in the centre of the pole figure. There is no indication of the former preferred orientation. The recalculated pole figures (Fig. 3*b*) and the related sigma sections (Fig. 4*a*) as well as the modelled pole figures (Fig. 3*c*) and sigma sections (Fig. 4*b*) confirm this interpretation.

Pyrite from Degtiarka

The polycrystalline material (PN-6) from Degtiarka, Central Ural Mountains, Russia (Zavaritsky, 1948) was provided by P. Natale (see Natale, 1971). The specimen cylinders were drilled at random because no layering was detectable. The grain fabric is similar to that of the Mt. Lyell ore with the exception that the grain size is more than twice the size of the pyrite of Mt. Lyell. Again the three (200)-, (220)- and (111)-pole figures were used to calculate a MENTEX-ODF (see Table 2). Fig. 5*a* shows the experimental, Fig. 5*b* the calculated pole figures, and Fig. 6*a* the ODF in projections perpendicular to the axis of an undeformed specimen. The main features of the pole figures are two fibre components. In the (100)-pole figure a (100)-maximum is located approximately 35° away from the specimen axis. A great circle distribution of (100)-poles occurs at 90° to this maximum. The maximum in the (111)-pole figure is also situated approx. 35° away from the specimen axis, but 45° from the <100>-fibre axis. The presence of this <111>-fibre axis is interpreted to give rise to the weak, small circle distribution of (100)-poles 55° away from the <111>-fibre axis. The model pole figures (Fig. 5*c*) and the related ODF (Fig. 6*b*) closely resemble the measured pole figures and confirm this interpetation.

This pyrite has been experimentally deformed by axial shortening at a strain rate of $2*10^{-4}\,s^{-1}$, a temperature of 600 °C of 300 MPa confining pressure (RUN 092). After yielding at 200 MPa, continuous work hardening occurred up to a flow stress of about 450 MPa at 24% strain. The development of weakly elongate grain fabrics, lattice bending and the progressive strain hardening in this sample indicate that deformation has involved dislocation flow processes. Fine grained, dynamically recrystallised grains developed locally along grain boundaries. Intragranular microcracking that is clearly related to Hertzian loading, has also occurred. The localised presence of diamond grain-shapes and long, planar grain-boundary segments, indicates that shortening may also have involved intergranular translation, by either frictional or ductile sliding processes. Fig. 7*a* shows the pole figures of the (200)-, (220)- and (111)-reflections which are projected in the same orientation as the pole figures of the undeformed specimen. The pole figures exhibit a preferred orientation which seems to be very similar to the undeformed material. The two fibre

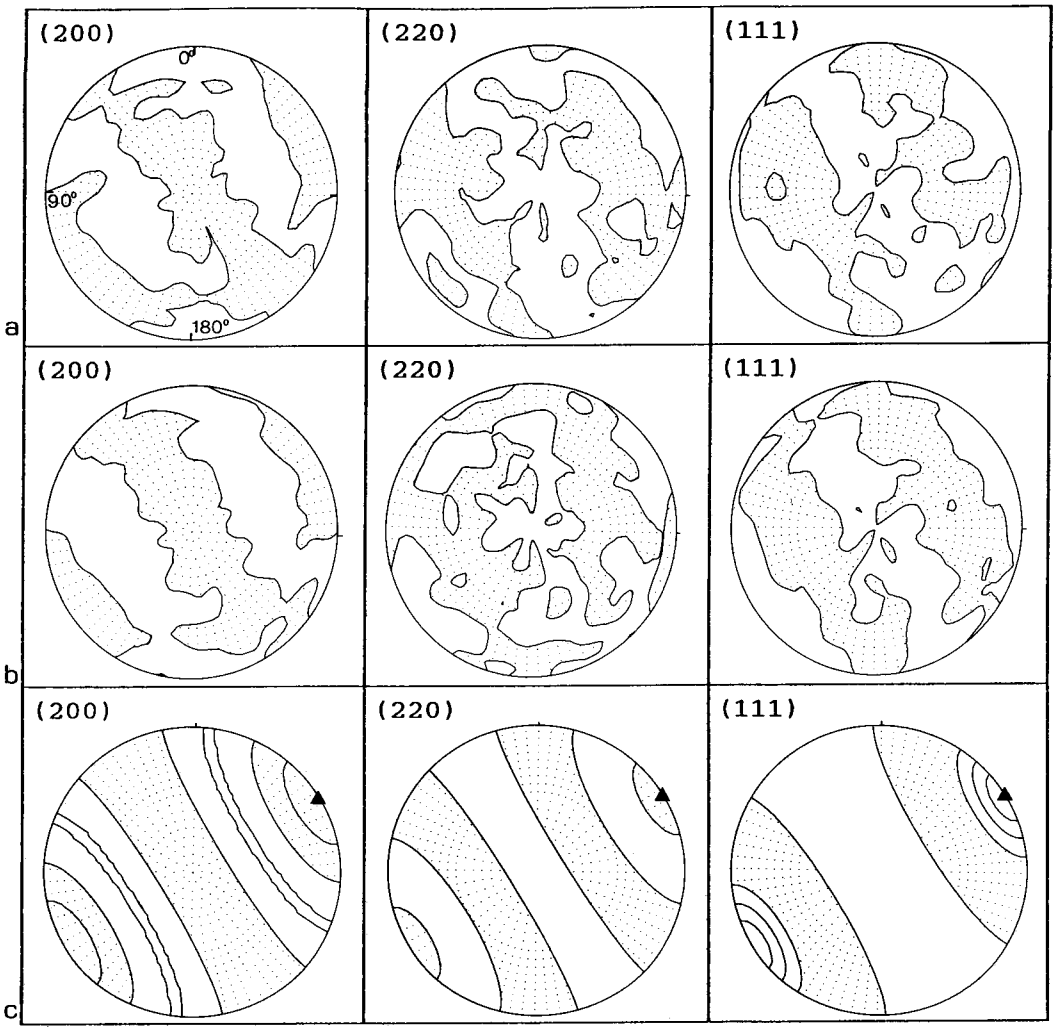

FIG. 1. Experimentally undeformed pyrite from Mt. Lyell, Tasmania (B-1), pole figures of the (200)-, (220)-, and (111)-reflections, equal area projection perpendicular to the shortening axis, dotted area: below 1.0 m.u.d., contour interval: 0.2. (*a*) measured pole figures; (*b*) recalculated pole figures (*c*) model pole figures: ▲ = <111>-fibre axis.

components that are present in the undeformed material are still there, but two new components have developed (Fig. 7*b,c*). The first one is also a fibre component with a (111)-maximum very close to the specimen axis and the second one is a <110>-fibre with the maximum in the specimen axis. The sigma sections of the calculated ODF (Fig. 8*a*) in comparison to the model ODF (Fig. 8*b*) confirm this interpretion.

Discussion

The interpretation of the measured textures is complicated firstly by the fact that the undeformed samples already have a weak preferred orientation. Secondly, after 24% shortening (for B-1) and 30% shortening (for PN-6) the new textures are still very weak. In deformation experiments with other cubic minerals under conditions in which dislocation glide is the dominant deformation mechanism, the newly developed preferred orientations are much sharper and often already well recognizable after 5% strain. After 10 to 20% strain the maxima often have densities of the order of 2 m.u.d. (see e.g. Kollenberg and Siemes, 1983; Siemes, 1976).

Lattice preferred orientation of naturally deformed pyrite. Although the naturally

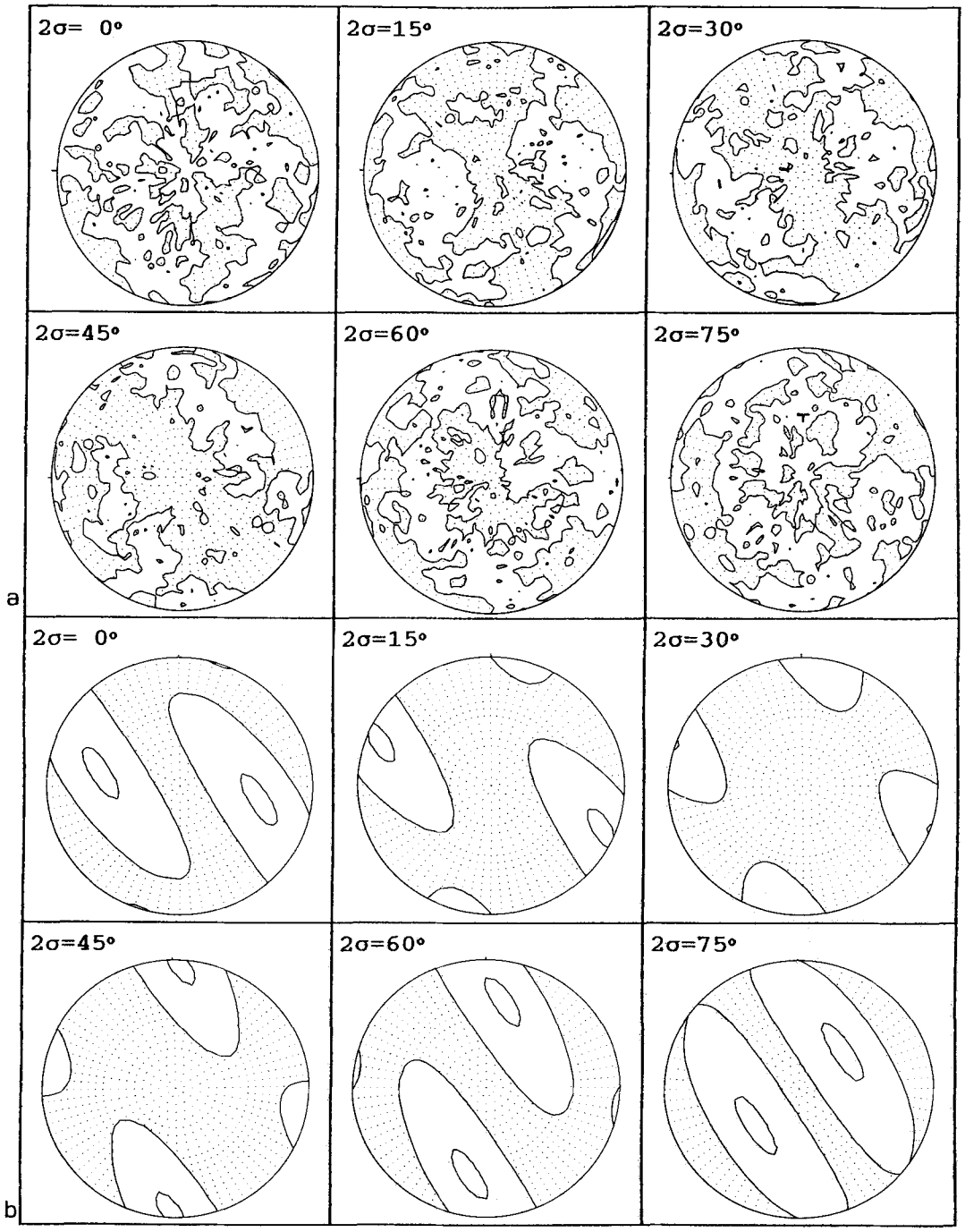

FIG. 2. Experimentally undeformed pyrite from Mt. Lyell, Tasmania (B-1), ODF-sigma-sections, dotted area: below 1.0 m.u.d., contour interval: 0.5. (*a*) calculated ODF after 22 interations; (*b*) model ODF.

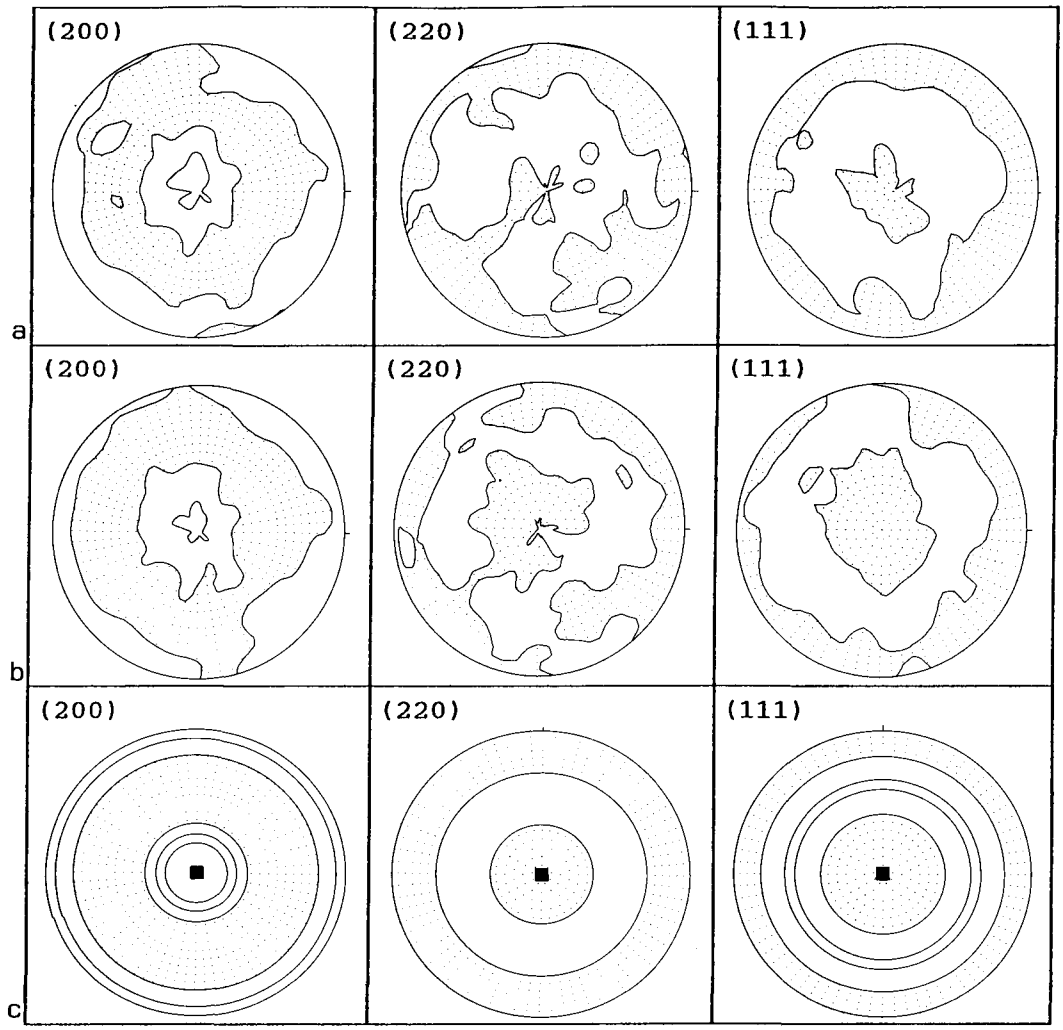

FIG. 3. Experimentally deformed pyrite from Mt. Lyell, Tasmania (RUN 053), pole figures of the (200)-, (220)-, and (111)-reflections, equal area projection perpendicular to the shortening axis, dotted area: below 1.0 m.u.d., contour interval: 0.2. (*a*) measured pole figures; (*b*) recalculated pole figures; (*c*) model pole figures, ■ = <100>-fibre axis.

deformed pyrite ores from Mt. Lyell and Degtiarka have weak preferred orientations, fibre textures are clearly recognisable. The <111>-fibre texture in the Mt. Lyell pyrite is perpendicular to the grain-size banding in the ore and is similar to the texture of polycrystalline pyrite from Bayerland (Gehlen, 1971). The microfabric of the Mt. Lyell pyrite has developed during deformation and recrystallisation at low metamorphic grades. The pyrite locally has a grain elongation fabric parallel to the grain-size banding. An extremely low dislocation density in the B-1 pyrite, together with truncation and overgrowth features on internal growth zones in the elongate pyrite, indicate that the Mt. Lyell pyrite ore has been deformed predominantly by dissolution-precipitation creep processes (Cox, 1987).

The lattice preferred orientation of the Degtiarka pyrite differs from that of the B-1 pyrite in that a distinct <100>-fibre texture is present, together with a weaker <111>-fibre. In view of the microstructural evidence (Natale, 1971; Couderc *et al.*, 1980), the development of the lattice preferred orientation in the Degtiarka pyrite is interpreted to have involved dislocation flow processes. However, the complexity of the fabric indicates that the strain history may have involved a non-coaxial deformation path.

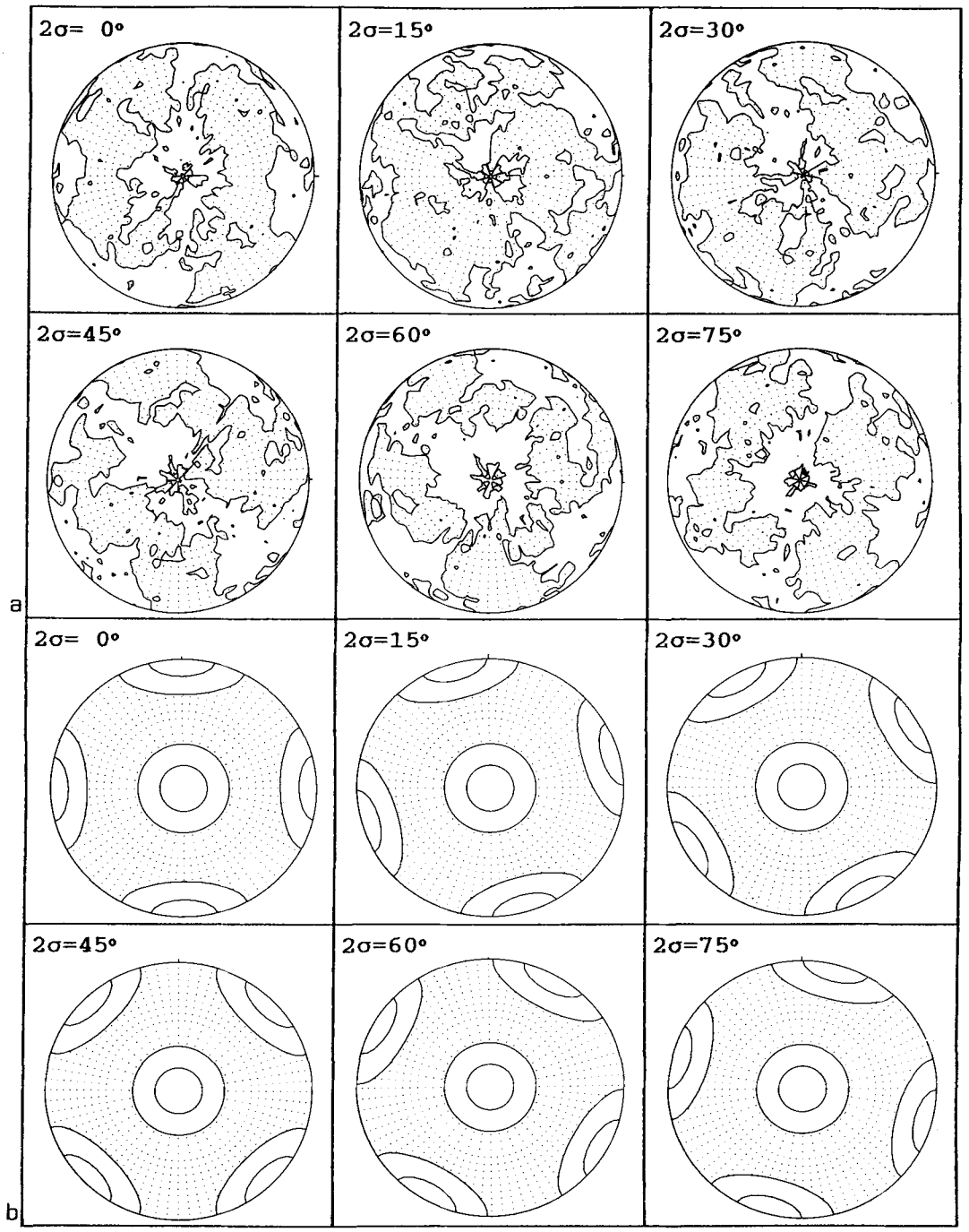

FIG. 4. Experimentally deformed pyrite from Mt. Lyell, Tasmania (RUN 053), ODF-sigma-sections, dotted area: below 1.0 m.u.d.; contour interval; 0.5. (*a*) calculated ODF after 22 iterations; (*b*) model ODF.

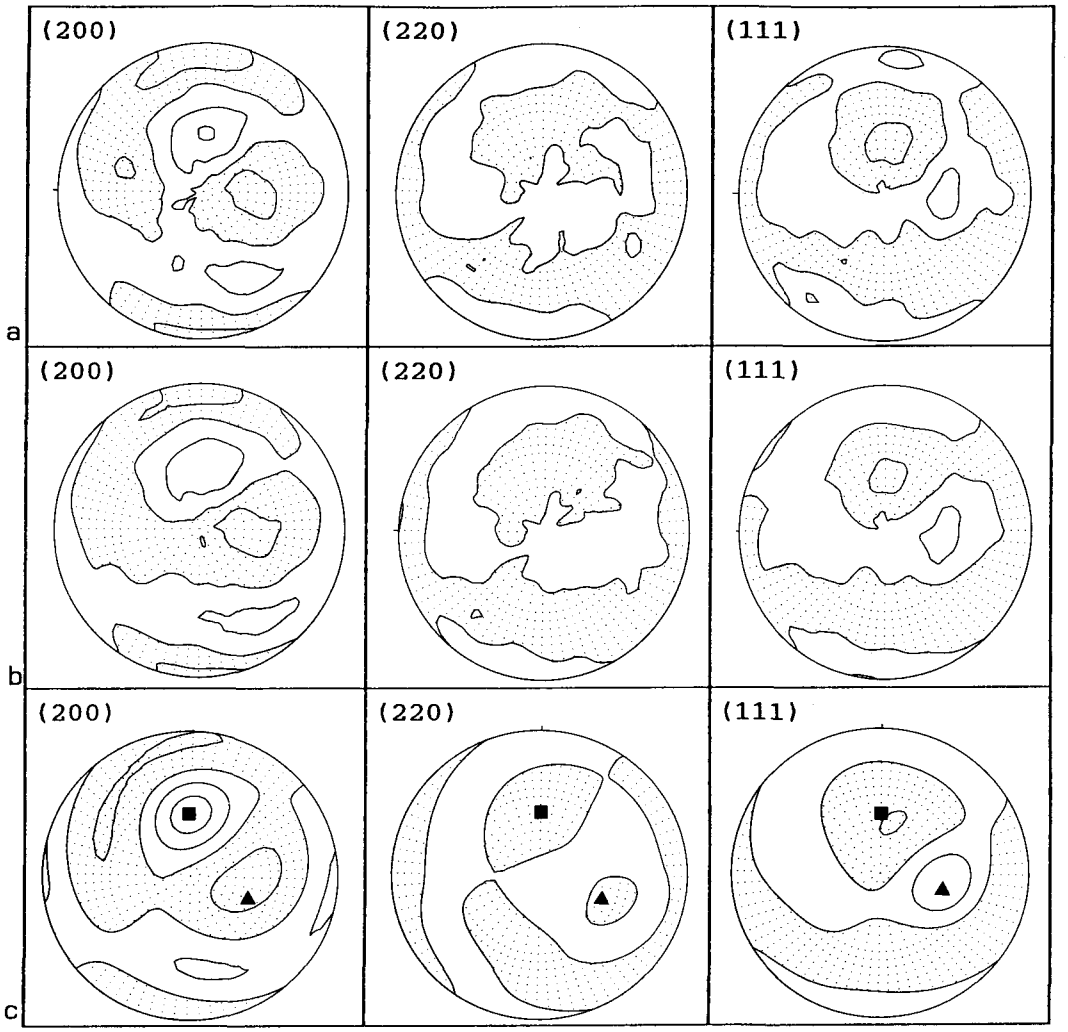

FIG. 5. Experimentally undeformed pyrite from Degtiarka, Ural (PN-6), pole figures of the (200)-, (220)-, and (111)-reflections, equal area projection perpendicular to the shortening axis, dotted area: below 1.0 m.u.d., contour interval: 0.2. (*a*) measured pole figures; (*b*) recalculated pole figures; (*c*) model pole figures; ▲ = <111>-fibre axis, ■ = <100>-fibre axis.

Lattice preferred orientations in experimentally deformed pyrite. The interpretation of the measured lattice preferred orientations in the experimentally deformed pyrite polycrystals is complicated by several factors. Firstly, the fabrics in the experimentally deformed materials are quite weak, even after 24% shortening (for B-1) and 30% shortening (for PN-6). Additionally, the starting materials have distinct initial lattice preferred orientations. As the initial fabrics have only been investigated in two small specimens, the variability of the fabrics in the B-1 and Pn-6 pyrite has not been evaluated. Accordingly, direct comparisons between the measured initial fabrics and the fabrics of the deformed specimens are subject to some uncertainty. Clearly, in future work on such weak lattice preferred orientations, it would be desirable to use the neutron diffraction technique to measure the lattice preferred orientation of the total specimen volume both before and after deformation.

The two specimens have been deformed at different temperatures whereas the other conditions were approximately the same. The Degtiarka ore had been deformed at 600 °C just above the temperature at which dynamic recrystallisa-

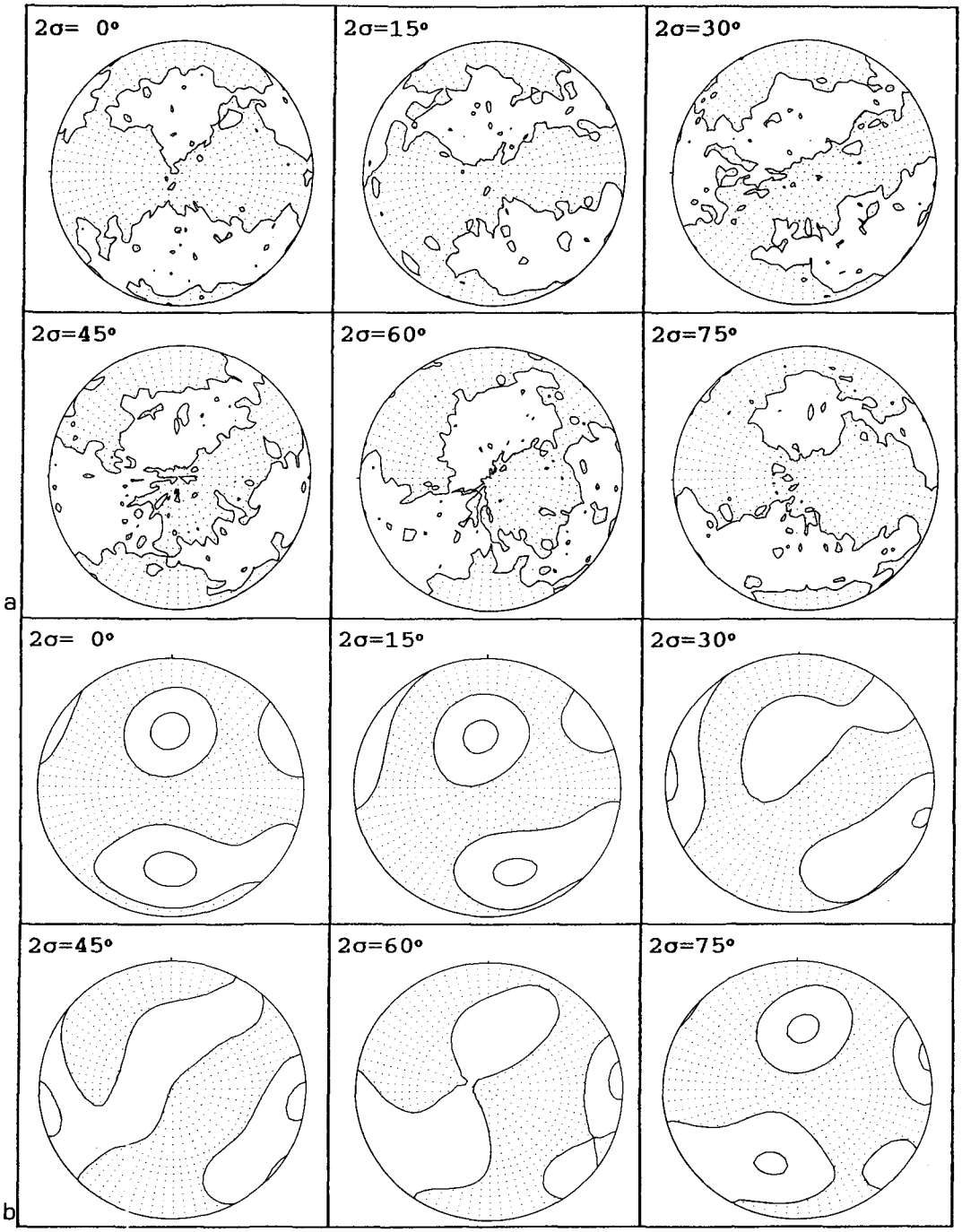

FIG. 6. Experimentally undeformed pyrite from Degtiarka, Ural (PN-6). ODF-sigma-sections, dotted area: below 1.0 m.u.d., contour interval: 0.5. (*a*) calculated ODF after 22 interations; (*b*) model ODF.

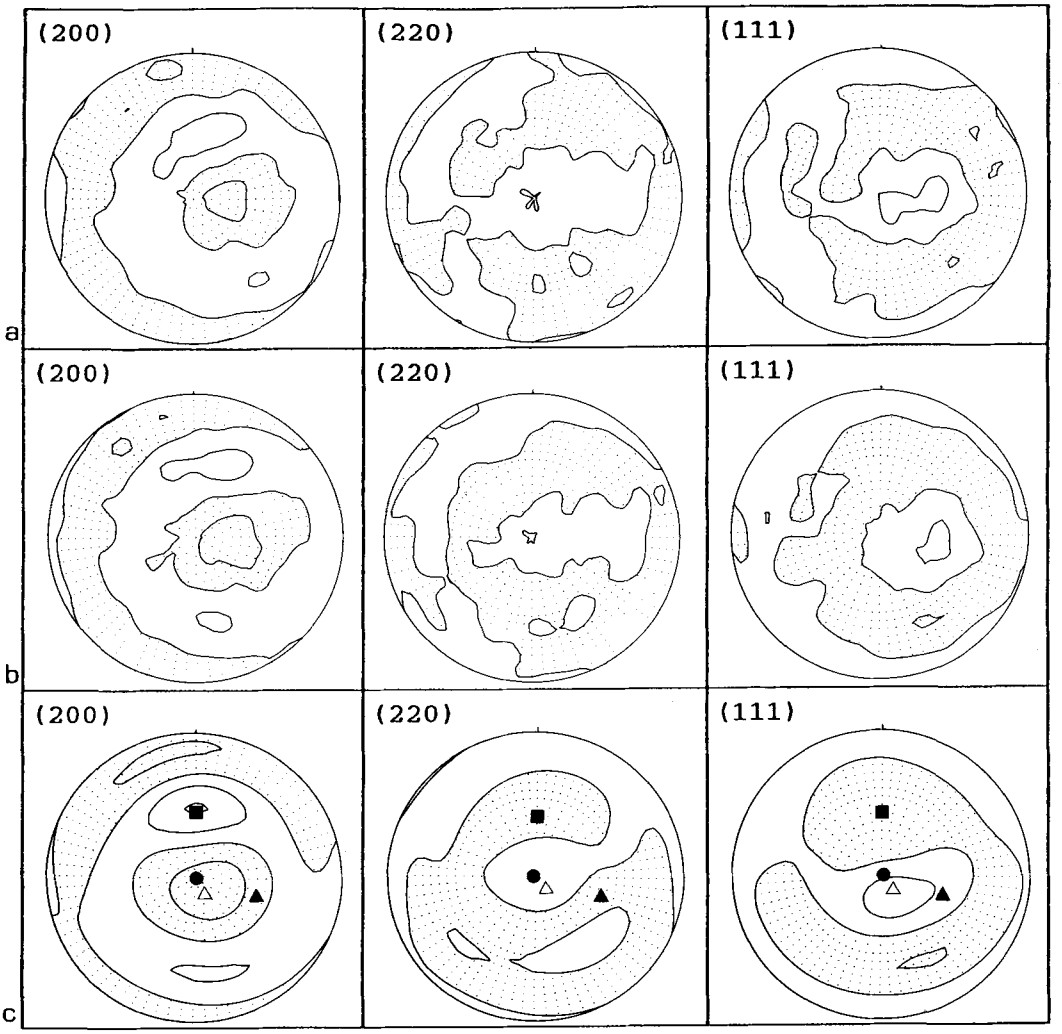

FIG. 7. Experimentally deformed pyrite from Degtiarka, Ural (RUN 092), pole figures of the (200)-, (220)-, and (111)-reflections, equal area projection perpendicular to the shortening axis, dotted area: below 1.0 m.u.d., contour interval: 0.2. (*a*) measured pole figures; (*b*) recalculated pole figures; (*c*) model pole figures; △ and ▲ = <111>-fibre axes, ■ = <100>-fibre axis, ● = <110>-fibre axis.

tion processes begin. However, the stress strain curve shows strong strain hardening. The development of a <110>-fibre texture in the experimentally deformed Degtiarka pyrite is similar to the response of many other cubic minerals. However the development of the <111>-fibre component has never been observed in other cubic minerals. Additional experiments are necessary to establish whether this component of the fabric is inherited from the starting material, or is purely a response to the dislocation glide systems operative in pyrite at 600 °C. The Mt. Lyell ore has been deformed at 700 °C without strain hardening under conditions where dynamic recrystallisation has been important during dislocation creep. The newly developed <100>-fibre might therefore be characteristic for these conditions. It is certainly remarkable that this fibre is a component in the natural Degtiarka ore.

Conclusions

Neutron diffracion techniques have been used successfully to detect weak lattice preferred orientations in naturally and experimentally deformed polycrystalline pyrite ores.

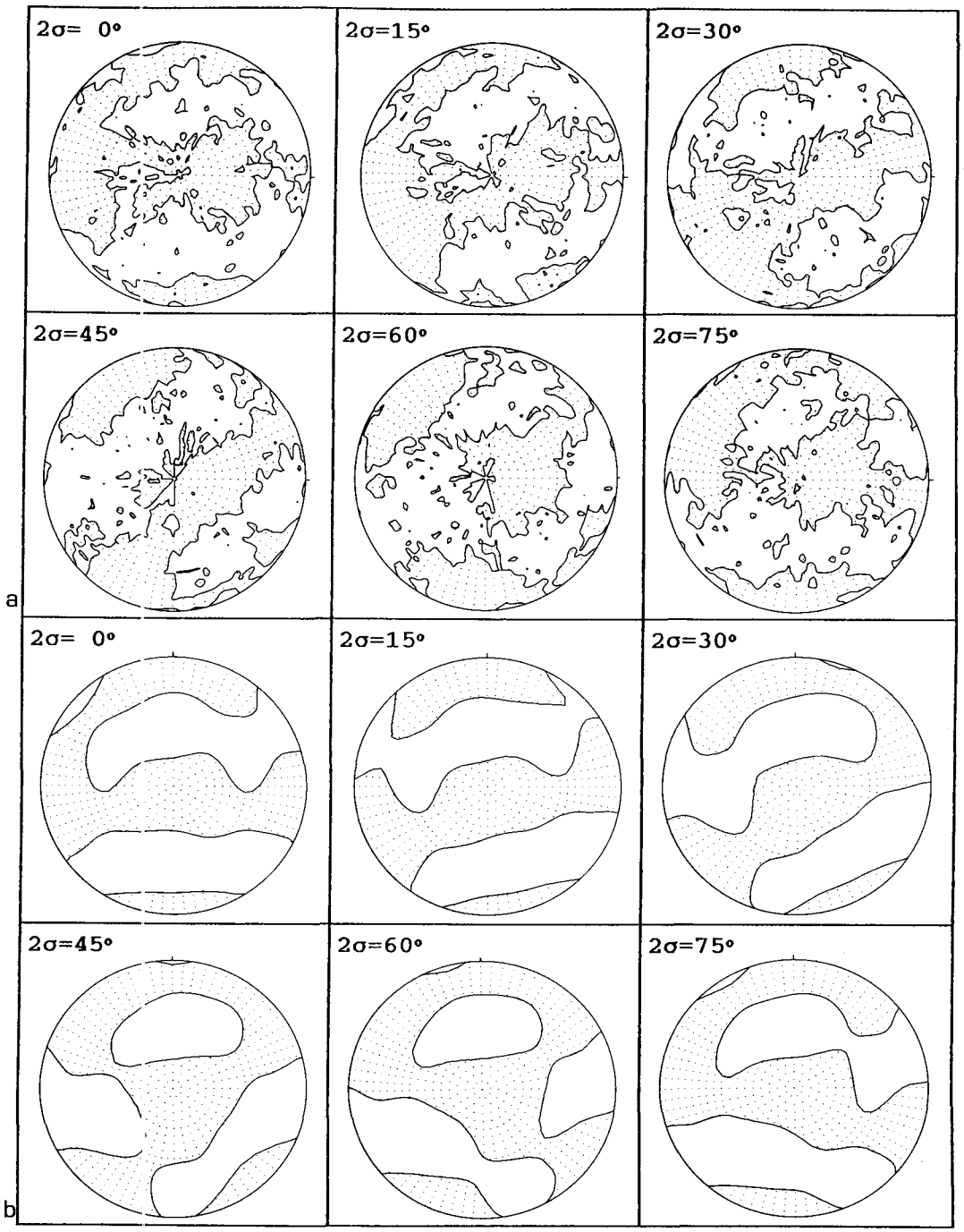

FIG. 8. Experimentally deformed pyrite from Degtiarka, Ural (RUN 092), ODF-sigma-sections, dotted area: below 1.0 m.u.d., contour interval: 0.5. (*a*) calculated ODF in sigma-sections; (*b*) model ODF.

The development of lattice preferred orientations during the experimental deformation of two polycrystalline pyrite ores supports earlier microstructural and mechanical evidence (Couderc *et al*, 1980; Cox *et al.*, 1981; Graf *et al.*, 1981; Levade *et al.*, 1982; Cox, 1987) that dislocation flow processes operate in pyrite at elevated temperatures and pressures. However, after 24% and 30% shortening of the samples, the lattice preferred orientations are unusually weak in comparison with those developed in other experimentally deformed cubic minerals. These fabrics have only been detected by means of neutron diffraction texture goniometry.

The weakness of the fabrics is interpreted to have been influenced by a number of factors including microcracking and intergranular sliding because of the apparently low number of independent slip systems during specimen shortening. The development of <110>- and <111>-fibre textures in the 600 °C experiment contrasts with the development of a <100>-fibre texture in the 700 °C experiment, and may indicate a change in the dominant flow mechanism with changing temperature.

Additional experiments are necessary to assess more clearly the development of lattice preferred orientations during the high-temperature deformation of polycrystalline pyrite, and especially to examine the possibility that fabric transitions occur in response to changes in dominant slip systems with changing temperature. In view of the weakness of the fabrics in pyrite, the use of neutron diffraction techniques has a number of advantages relative to X-ray diffraction techniques for fabric analysis. In particular, the application of neutron diffraction techniques will allow the measurement of the lattice preferred orientation of the total sample volume both before and after deformation.

Acknowlegements

SFC acknowledges the support of a CSIRO Postdoctoral Fellowship when the deformation experiments were orginally performed in the Department of Earth Sciences at Monash University. The Degtiarka pyrite was supplied by P. Natale. Computing was done with an IBM3090 at the computer centre of the Aachen Technical University (RWTH). The critical comments of the referees especially of G. E. Lloyd contributed to the improvement of this publication.

References

Barrett, C. S. and Levenson, L. H. (1940) Trans. AIME 137 (1940) 112–127, cited in Mecking, H. (1985) Textures of Metals. In *Preferred Orientation in Deformed Metals and Rocks: An Introduction to Modern Texture Analysis* (Wenk, H.-R., ed.). Academic Press Orlando, Ch. 13, 267–306.

Bunge, H. J. (1985) Representation of Preferred Orientations. Ibid., Ch. 4, 73–108.

——and Esling, C. (1985) The Harmonic Method. Ibid., Ch. 5, 109–22.

Carter, N. L. and Heard, H. C. (1970) Temperature and rate dependent deformation of halite. Am. J. Sci. **269**, 193–249.

Couderc. J.-J., Bras, J., Fagot, M., and Levade, C. (1980) Etude par microscopic electronic en transmission de le'etat de deformation de pyrite de differentes provenances. *Bull. Mineral.* **103**, 547–57.

Cox, S. F. (1987) Flow Mechanism in Sulphide Minerals. In *Mechanical and Chemical (Re)mobilisation of Metalliferous Mineralisation* (Marshall, B. and Gilligan, L. B., eds.). *Ore Geology Rev.* **2**, 133–71.

——Etheridge, M. A., and Hobbs, B. E. (1981) The Experimental Ductile Deformation of Polycrystalline and Single Crystal Pyrite. *Econ. Geol.* **76**, 2105–17.

Foitzik, A., Skrotzki, W., and Haasen, P. (1991) Slip on {111} planes in lead sulphide. Materials Sci. Engin., **A132**, 77–82.

Gehlen v., K. (1971) X-Ray Analysis of Preferred Orientation of Ore Minerals—in Particular with the Pole-figure Goniometer. *Siemens Rev., 5th Spec. Issue,* **38**, 45–64.

Graf, J. L., Skinner, B. J., Bras, J., Fagot, M. Levade, C. and Couderc, J.-J. (1981) Transmission Electron Microscope Observation of Plastic Deformation in Experimentally Deformed Pyrite. *Econ. Geol.* **76**, 738–42.

Kämpf, H., Ertel, A., Bankwitz, P., Betzl, M., and Zänker, G. (1987) Texturanalyse an Evaporiten der Lagerstätte Zielitz-Nachweis einer Fasertextur in Halititen. *Zeitschr. angew. Geol.* **33**, 104–7.

Kelly, A. and Groves, G. W. (1970) *Crystallography and Crystal Defects,* Longman London, p. 428.

Kern, H. and Braun, G. (1973) Deformation und Gefügeregelung von Steinsalz im Temperaturbereich 20–200 °C. *Contrib. Mineral. Petrol.* **40**, 169–81.

——and Richter, A. (1985) Microstructures and Textures in Evaporites. In *Preferred Orientation in Deformed Metals and Rocks: An Introduction to Modern Texture Analysis* (Wenk, H.-R., ed.). Academic Press Orlando, Ch. 15, 317–33.

Kollenberg, W. and Siemes, H. (1983) Experimental Deformation of a Sphalerite-Garnet Ore under a Confining Pressure of 300 MPa and at Temperatures between 25 °C and 300 °C, In *Deformation of Multi-Phase and Particle Containing Materials, Proc. 4th Riso Int. Symp. on Metallurgy and Materials Science* (J. B. Bilde-Sorensen, N. Hansen, A. Horeswell, T. Leffers and H. Lilholt, eds.), 351–6.

Lang, H. (1968) *Stauchversuche mit polykristallinen Kupferkiesen und deren Ergebnisse unter besonderer Berücksichtigung der Gefügeregelung.* Dissertation RWTH Aachen.

Levade, C., Couderc, J.-J., Bras, J. and Fagot, M. (1982) Transmission Electron Microscopy Study of Experimentally Deformed Pyrite. *Philos. Mag.* **A46**, 307–325.

Matthies, S. (1991) On the Principle of Conditional Ghost Correction and its Realisation in Existing Correction Concepts. *Textures and Microstructures,* **14–18**, 1–12 (Special Issue: Ninth Int. Conf. Text. Mat. (Icotom 9), Avignon 1990, Eds. Esling, C. and Penelle, R.).

——Vinel, G. W., and Helming, K. (1987) *Standard Distributions in Texture Analysis, Maps for the Case of Cubic-Orthorhombic Symmetry.* Akademie Verlag Berlin, Vol. 1, p. 442.

——Helming, K., Steinkopff, T., and Kunze, K. (1988*a*) Standard Distributions for the Case of Fibre Textures. *Phys. Stat. Sol. (b),* **150**, K1–K5.

——Vinel, G. W., and Helming, K. (1988*b*) *Standard Distributions in Texure Analysis, Maps for the Case of Cubic-Orthorhombic Symmetry.* Akademie Verlag Berlin, Vol. 2, p. 256.

——Helming, K., and Kunze, K. (1990*a*) On the Representation of Orientation Distributions in Texture analysis by σ-Sections, I. General Properties of σ-Sections: *Phys. Stat. Sol. (b),* **157**, 71–83, II. Consideration of Crystal and Sample Symmetry, Examples. Ibid., **157**, 489–507.

——Vinel, G. W. and Helming, K. (1990*b*) *Standard Distributions in Texture Analysis, Maps for the Case of Cubic-Orthorhombic Symmetry.* Akademie Verlag Berlin, Vol. 3, p. 480.

Mises v., R. (1928) Mechanik der plastischen Formänderung von Kristallen. *Z. Angew. Math. Mech.,* **8**, 161–85.

Müller, P. and Siemes, H. (1972) Zur Festigkeit und Gefügeregelung von experimentell verformten Magnetiterzen. *Neues Jahrb. Mineral., Abh.*, **117**, 39–60.

Natale, P. (1971) Prima segnalazione de strutture de deformazione plastica della pirite. *Rend. Soc. Mineral. Petrol. Ital.* **27**, 537–50.

Pawlik, K., Pospiech, J. and Lücke, K. (1991) The ODF Approximation from Pole Figures with the Aid of the ADC Method. *Textures and Microstructures,* **14–18,** 25–30 (Special Issue: Ninth Ont. Conf. Text. Mat. (Icotom 9), Avignon 1990, Eds. Esling, C and Penelle, R.)

Pratt, P. L., Roy, C. and Evans, A. G. (1966) The Role of Grain Boundaries in the Plastic Deformation of Calcium Fluoride, in *Materials Science Research,* Vol. 3: *The Role of Grain Boundaries and Surfaces in Ceramics* (Kriegel, W. W. and Palmour III, H., eds.), Plenum Press New York, Ch. 14, 225–41.

Saynisch H. J. (1970) Festigkeits- und Gefügeuntersuchungen an experimentell und natürlich verformten Zinkblendeerzen. In *Experimental and Natural Rock Deformation* (P. Paulitsch, ed.). Springer Verlag, Berlin, 209–52.

Schaeben, H. (1988) Entropy Optimisation in Texture Goniometry, I. Methodology. *Phys. Stat. Sol. (b),* **148**, 63–72.

——(1991) Entropy Optimisation in Quantitative Texture Analysis. II Application to Pole-to-Orientation Density Inversion. *J. Appl. Phys.*, **69**, 1320–9.

——and Siemes, H. (1991) Recovering ODF's with Maximum Entropy and their Geoscientific Interpretation. *Textures and Microstructures,* **14–18**, 31–36 (Special Issue: Ninth Int. Conf. Text. Mat. (Icotom 9), Avignon 1990, Eds. Esling, C and Penelle, R.)

——and Auerbach, S. (1990) Entropy Optimisation in Texture Goniometry, II. Practical Applications. *Phys. Stat. Sol. (b),* **158**, 407–25.

Siemes, H. (1970) Experimentelle Verformung von Bleiglanzerzen. In *Experimental and Natural Rock Deformation* (P. Paulitsch, ed.). Springer Verlag, Berlin, 165–208.

——(1976) Recovery and Recrystallisation of Deformed Galena, *Econ. Geology,* **71**, 763–71.

——and Hennig-Michaeli, Ch. (1985) Ore Minerals. In *Preferred Orientation in Deformed Metals and Rocks: An Introduction to Modern Texture Analysis* (Wenk, H.-R., ed.). Academic Press Orlando, Ch. 16, 335–60.

Vadon, A. and Heizmann, J. J. (1991) A New Program to Calculate the Texture Vector of the Vector Method. *Textures and Microstructures* **14–18**, 37–44 (Special Issue: Ninth Int. Conf. Text. Mat. (Icotom 9), Avignon 1990, Eds. Esling, C. and Penelle, R.)

Will, G., Schäfer, W., and Merz, P. (1989) Texture Analysis by Neutron Diffraction Using a Linear Position Sensitive Detector. *Textures and Microstructures,* **10**, 375–87.

Zavaritsky, A. N. (1948) Metasomatism and Metamorphism in the Pyrite Deposits of the Urals. *XVIII Int. Geol. Congress, London,* Sect. B, Part III, 102–108.

Zilles, D. (1989) *Texturuntersuchungen und mikroskopische Charakterisierung von experimentell verformten polykristallinen Pyrit-Erzen.* Diplomarbeit RWTH Aachen, unpubl., 105 p.

[*Manuscript received 22 January 1992: revised 29 June 1992*]